Copper−Carbon Cluster CuC_3: Structure, Infrared Frequencies, and Isotopic Scrambling

Jan Szczepanski, Yun Wang, and Martin Vala*

Department of Chemistry and Center for Chemical Physics, University of Florida, Gainesville, Florida 32611-7200

Received: February 6, 2008; Revised Manuscript Received: March 13, 2008

Copper−carbon clusters, formed by dual Nd/YAG laser vaporization, have been trapped in solid Ar at 12 K and investigated by infrared spectroscopy. Density functional calculations of a number of possible molecular structures for Cu/carbon clusters have been performed, and their associated vibrational harmonic mode frequencies and dissociation energies have been determined with a 6−311++G(3df) basis set using both B3LYP and MPW1PW91 functionals. Both computations and ^{13}C-isotopic substitution experiments indicate that new bands observed at 1830.0 and 1250.5 cm^{-1} are due to the asymmetric and symmetric C═C stretching modes, respectively, in the near-linear CuC_3 ($X\,^2A'$) cluster. Photoinduced $^{12/13}C$-isotopic scrambling in $Cu^{12/13}C_3$ clusters has also been observed. The mechanism for the photoscrambling is shown to involve the formation of a bicyclic CuC_3 isomer.

1. Introduction

Transition metals may be important components in the chemistry of the interstellar medium. Iron, with its high nuclear stability, is the most abundant metal in interstellar space, but despite its abundance, it is known to be depleted about 100-fold compared with our solar system. Complexation of iron with polycyclic aromatic hydrocarbons (PAHs) and/or carbon clusters has been proposed as the reason for this depletion.[1–4] Other transition metals are also present in the interstellar medium, although at lower concentrations.[3,5] Their participation in interstellar chemistry is largely unknown, primarily because of a dearth of information on their spectral properties. However, recent studies by Graham and Rittby and co-workers on the infrared spectroscopy of matrix-isolated transition metal−C_3 clusters, such as linear GeC_3Ge, fanlike TiC_3, linear CrC_3 and CoC_3, and floppy NiC_3Ni have begun to provide some of this much-needed information.[6–10]

Using satellite-based measurements, Jenkins et al. analyzed Cu^+ ion column densities along various lines of sight for early type stars and found a substantial depletion of Cu^+ compared with our solar system.[3] Laboratory studies of copper reactivity with interstellar molecules such as carbon clusters are therefore important initial steps in understanding its interstellar chemistry. In this paper, we report our laboratory study on the formation of Cu−carbon clusters and present evidence for the existence of CuC_3.

Previous laboratory work on copper−carbon clusters has been limited. Cationic CuC_n^+ clusters ($n = 1-3$), generated in spark discharges of Cu and graphite, have been observed in mass spectrometric studies.[11] Copper acetylide (CuC≡CCu) has been formed by the reaction of acetylenic compounds with copper salts in liquid ammonia[12] and is widely used as a catalyst in the production of copper powder.[13] Other CuC_n compounds, including copper acetylide, have been observed in oxyacetylene/hydrogen/copper flames.[14] Time-of-flight mass spectrometric studies of Cu−C metallo-carbohedrenes ("met-cars") identified the clusters $Cu_nC_2^+$ ($n = 2k + 1$, $k = 1-7$) and $Cu_nC_4^+$ ($n = 2k + 1$, $k = 2-4$) and speculated on their possible structures.[15]

* Author to whom correspondence should be addressed. E-mail: mvala@chem.ufl.edu.

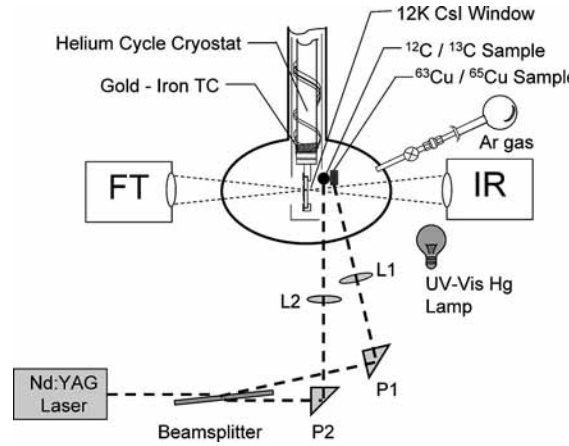

Figure 1. Experimental setup for generation and trapping of the copper−carbon clusters trapped in solid Ar at 12 K. Two focused laser beams with adjustable intensities ablate the copper and pressed powder ^{12}C (and ^{13}C) mixture. The reaction products (mixed with Ar gas) are frozen on an IR-transparent CsI window to form a matrix and are probed using a Fourier transform infrared (FT-IR) spectrometer.

In this paper, we report on a matrix-isolation infrared spectroscopic study of laser-ablated Cu−carbon clusters and corresponding theoretical work on small stable copper−carbon systems, Cu_mC_n ($m = 1, 2$; $n = 1, 2, 3$). The equilibrium geometries, vibrational harmonic frequencies, and stabilities for these clusters have been calculated using density functional theory. When compared with our experimental data, these results show that only the CuC_3 cluster was observed in our experiments. Photoinduced $^{12/13}C$-isotopic scrambling in $Cu^{12/13}C_3$ isotopomers has also been observed and is proposed to occur via a bicyclic CuC_3 intermediate.

2. Experimental Methods

The experimental apparatus used for the generation and trapping of copper−carbon clusters in solid Ar is shown in Figure 1. The output from a pulsed Nd:YAG laser (1064/532 nm, 0.2−0.5 W, 10 Hz) was split into two beams, with one beam (intensity ca. 60%) directed by prism P1 and focused by lens L1 to an ~0.5 mm diameter spot on a piece of Cu metal

10.1021/jp801111m CCC: $40.75
Published on Web 05/06/2008

(SPEX, natural abundance: ^{63}Cu (69.2%) and ^{65}Cu (30.8%)). The second beam (intensity ca. 40%) was focused to a 2−3 mm diameter spot on a pressed pellet of ^{12}C and ^{13}C (ISOTEC). The Cu and C samples, approximately 4−5 mm apart, were positioned close to the CsI sample window. By rotating the glass plate beam splitter, the ratio of the intensity of the reflected beam to the intensity of the transmitted beam could easily be changed. With an ∼80° angle of incidence, the intensities of the reflected and transmitted beams are equal, as expected from the Fresnel formula.[16] Both L1 and L2 lenses were mounted on micrometer screw-driven mounts which allowed for periodic repositioning of the focused laser beams onto fresh regions of the carbon and copper samples.

Infrared spectra were scanned using a NICOLET Magna 560 FT-IR spectrometer (0.5 cm^{-1} resolution) after a 2−3 h deposition of the Cu/C_n/Ar mixture on a CsI sample window held at 12 K by a closed-cycle helium cryostat (APD Displex). Annealing to 35 K followed by recooling to 12 K, as well as photolysis with a medium pressure 100 W Hg lamp, was used as needed to induce secondary reactions.

3. Computational Methods

Calculation of molecular equilibrium geometries and associated vibrational harmonic mode frequencies and dissociation energies were calculated using density functional theory with the Gaussian 03 program package[17] using Becke's three-parameter hybrid functional combined with the nonlocal correction functional of Lee, Yang, and Parr (B3LYP)[18] and a 6−311++G (3df) basis set which contains three sets of d functions and one set of f functions.

For systems containing transition metals, the B3LYP functional has been shown to occasionally predict incorrect equilibrium geometries, as determined by a comparison of experimental and calculated vibrational spectra.[19–22] So, in addition, we used the MPW1PW91 functional, a modified Perdew−Wang exchange and correlation functional, along with a 6−311++G(3df) basis set to verify the B3LYP optimized structure.[23,24] This approach has been recommended by Wiberg,[19] Dunbar,[20] and Oomens et al.[21] in their studies of C, H, and metal-containing systems. The MPW1PW91 functional was used in our recent studies of iron complexed with cationic and neutral polycyclic aromatic hydrocarbons.[4,22]

We also tested the BPW91 functional (on the near-linear CuC_3 cluster) by using the 6−311++G(3df) basis set for the carbons and SDD pseudopotential for copper. Such a functional has been recommended for copper, silver, and gold[25] and has been used in calculations of various reaction products of these metals with hydrogen.[26]

From our $^{63}Cu^{12/13}C_3$ isotopomer frequency calculations (BPW91/6−311++G(3df)[carbons]/SDD pseudopotential [Cu]), we find that the maximum difference (after scaling) between predicted and observed vibrational frequencies is large, 7.3 cm^{-1}, but this value drops to 2.4 cm^{-1} when the MPW1PW91 functional is used with the same basis sets. Finally, when the MPW1PW91 functional and the 6−311++G(3df) basis set is used for all atoms, this maximum difference drops to 1.6 cm^{-1}, an acceptable value for ^{13}C labeling assignments.

The potential energy surface of the isomerization reaction for the near linear CuC_3 cluster was plotted using the MPW1PW91/6−311++G (3df) level of theory exclusively. The transition state (TS) identified from this plot was verified using traditional transition state optimization with the Berny optimization algorithm, as incorporated in the Gaussian 03 package.[17]

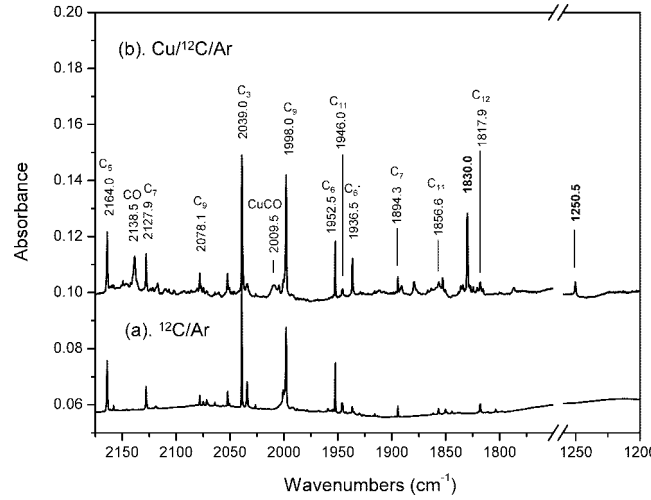

Figure 2. Infrared absorption spectra of products of laser ablation of graphite (spectrum a) and products of two-beam laser ablation of graphite and copper (spectrum b, enlarged twofold). The spectra were recorded after matrix annealing to 35 K then cooling back to 12 K. The major bands due to pure carbon clusters and their reaction products with copper at 1830 and 1250.5 cm^{-1} are indicated. Carbon monoxide and its product with copper are also marked.

4. Results and Discussion

4.1. Experimental Infrared Spectra. Figure 2 shows the infrared absorption spectra in the 1200−1260 cm^{-1} and 1750−2200 cm^{-1} ranges for species formed by the laser ablation of graphite (spectrum a) and by the synchronized dual laser ablation of copper and graphite (spectrum b). The majority of bands in spectrum a have previously been assigned to various neutral carbon clusters (C_3−C_{12}) by us and others.[27,28] Several bands in spectrum b, not due to neutral carbon clusters, such as the anionic clusters, C_5^- (1831.8 cm^{-1}) and C_6^- (1936.5 cm^{-1})[29,30] are also present; the C_5^- band is very weak and masked by the shoulder of the strong 1830.0 cm^{-1} band and is therefore not marked in the figure. Also present are impurities such as CO and H_2O, which are known to be more abundant when high laser ablation powers are used.[9] Additional reaction products are also seen, namely, CuCO (2009.5 cm^{-1})[31] and C_3H (1824.4 cm^{-1}).[32,33]

Two new bands in spectrum b at 1830.0 and 1250.5 cm^{-1}, not found in spectrum a, were found to be dependent on both copper and carbon concentrations. To determine whether these two bands belong to the same species, a large number of experiments were performed under different experimental conditions, for example, different Cu/C concentration ratios (using different ablating laser beam intensities), matrix annealing up to 35 K, and, finally, UV−visible photolysis (up to 1 h). We found that the ratio of the integral intensities of the 1830 and 1250.5 cm^{-1} bands is constant under these different conditions (and ≅ 5.7 ± 0.3), supporting the conclusion that both bands arise from a common carrier.

The results of isotopic (^{13}C) substitution are shown in Figure 3 (top panel, spectrum b). Inspection of the ^{13}C-labeled spectrum built on the 1830 cm^{-1} band reveals eight isotopomeric bands, (**a**−**h**). A very similar isotopomer band pattern was previously observed for near-linear $^{12/13}C_3{\cdot}H_2O$ complexes[34] and linear $^{12/13}C_3Cr$[8] and $^{12/13}C_3Co$[9] clusters. Such a band pattern is characteristic of the CC asymmetric stretching mode in linear or near-linear $^{12/13}C_3$ with one end bonded to a ligand. In the next section, we explore whether linear or near-linear CuC_3 clusters can account for these results.

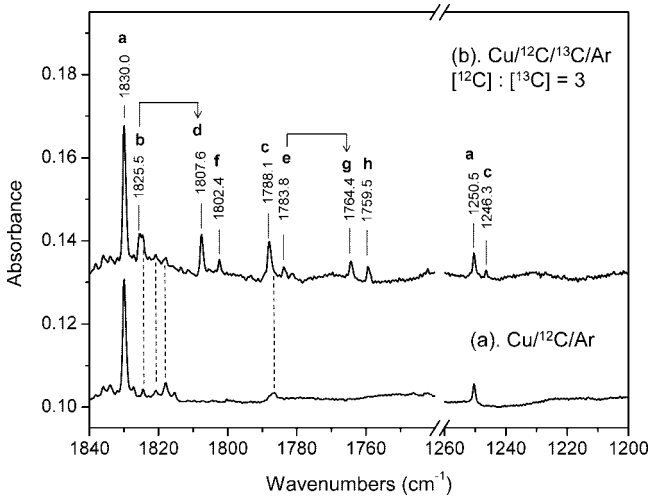

Figure 3. Infrared spectra of reaction products from laser ablation of Cu and ^{12}C (spectrum a) displayed in two energy regions. The bands at 1830.0 and 1250.5 cm^{-1} are due to a common carrier containing Cu and ^{12}C. Spectrum b was collected from runs similar to spectrum a, but with a ^{13}C-enriched sample. The band carriers marked by vertical dashed lines are due to C_3H (1824.4 cm^{-1}),[32,39] C_2H^+ (1820.2 cm^{-1}),[38] and C_{12} (1817.9 cm^{-1}).[39] The fractionations of **b** → **d** as well as of **e** → **g** isotopomers via the proposed $^{12/13}C$ isotopic scrambling in *nl*-$Cu^{12/13}C_3$ (see text) are marked.

4.2. Equilibrium Geometries and Vibrations for the Cu_mC_n ($m = 1, 2$ and $n = 1, 2, 3$) Clusters. Previous IR studies have identified metal−carbon clusters of the type MC_3 and MC_3M (M = transition metal atom).[6–10] Here, we explore such clusters theoretically for M = Cu and, in addition, explore the smaller MC, MC_2, and MC_2M species. Figure 4 shows the stable equilibrium geometries found for the Cu_mC_n clusters ($m = 1$, 2; $n = 1$, 2, 3) with displayed geometry and energy parameters predicted by MPW1PW91 and B3LYP functionals. Predicted harmonic vibrational frequencies and intensities are collected in Table 1. Total energies (corrected for zero point vibrational energies) and dissociation energies are given in Table 2.

4.2.1. CuC. MPW1PW91/6−311++G(3df) calculations predict that the lowest energy multiplet of diatomic CuC is a quartet with bond length = 1.817 Å. The doublet spin state is higher by 0.266 eV. B3LYP/6−311++G(3df) calculations find that the doublet state is only marginally higher (0.049 eV) than the quartet. Both theoretical levels predict very low vibrational integral intensities, 14 and 10 km/mol, respectively, which accounts for CuC not being observed in our experiments.

4.2.2. CuC_2. Our calculations predict that singlet dicarbon (C_2) reacts spontaneously with Cu ($X\ ^2S_{1/2}$) to form a doublet cyclic cluster, *c*-CuC_2 (structure **B**). The predicted Cu−C bond strength is 2.33 eV (2.47 eV) [B3LYP (MPW1PW91)], only slightly larger than that in quartet CuC, (1.99 eV (2.20 eV)). Table 1 shows that the strongest infrared mode in *c*-CuC_2 lies at 1750.3 cm^{-1} (1768.7 cm^{-1}; CC stretch), but since its calculated intensity is only 7 km/mol (5 km/mol), the absence of this band in our spectra is understandable.

4.2.3. Cu_2C. The lowest energy isomers of this cluster are triplets of **C** and **D**. The **D** (linear) isomer is higher in energy by 1.35 eV (MPW1PW91/6−311++G(3df)). The highest IR integral intensity for the more stable cyclic isomer **C** is only 7 km/mol and in an energy range inaccessible by our FT-IR.

4.2.4. Cu_2C_2. Copper acetylide, *l*-CuC_2Cu (**E**), is well-known in catalytic chemistry.[13] Predicted to appear at 662 cm^{-1}, this species is also absent in our spectra, presumably also because of its low concentration and intensity (65 km/mol). The second isomer *bc*-Cu_2C_2 (**F**) is higher in energy by 0.66 eV (Figure 3) and also has a very low IR intensity of 23 km/mol (Table 1).

4.2.5. CuC_3. Two stable structures were found for the CuC_3 cluster: near-linear, *nl*-CuC_3 (**G**), and bicyclic, *bc*-CuC_3 (**H**). The former is more stable by 0.64 eV (0.34 eV) in B3LYP (MPW1PW91) calculations (Table 2). The highest predicted band intensity for **H** is 25 km/mol for the 1595.8 cm^{-1} band. This species is not observed here.

The predicted CuC bond length in *nl*-CuC_3 (**G**) is 1.838 Å (1.825 Å), close to the experimental value of 1.8296 Å in CuCN.[35] Unscaled predicted vibrational frequencies (and integral intensities) for *nl*-CuC_3 are 1900.5 (172 km/mol; asymmetric CC stretch) and 1281.5 cm^{-1} (31 km/mol; symmetric CC stretch). The calculated (MPW1PW91) isotopomer frequencies for the CC asymmetric and symmetric modes in *nl*-$Cu^{12}C_3$ were scaled by factors (listed in Table 3) to match the observed 1830 and 1250 cm^{-1} bands. Although the MPW1PW91 predictions match experimental intensities [1830.0 (1.0) and 1250.5 (0.17) cm^{-1}], the B3LYP calculation fails to predict the correct intensity ratio for these bands (Table 1). The intensities predicted by B3LYP are 134 and 9 km/mol (1.0 and 0.067 relative intensities), respectively. The geometry predicted for **G** is substantially different using B3LYP versus MPW1PW91, especially for the CuCC angle, 153.0 versus 161.3°, respectively. In addition, some predicted mode symmetries are different for the two calculational levels, even though the structures and electronic ground states are the same (Table 1). The failure of the B3LYP functional for the **G** isomer is likely related to the large difference (0.3 eV) in predicted energy stability of the **G** and **H** isomers.

To confirm the assignment of the observed bands to the near-linear species, isotopic substitution experiments were run. Figure 3 shows bands due to the $^{12,13}C$ isotopomers built on the 1830.0 and 1250.5 cm^{-1} bands. Table 3 gives the comparison between the observed isotopomer bands and the predicted (and scaled) *nl*-$^{63}Cu^{12/13}C_3$ frequencies. The frequencies predicted by the MPW1PW91/6−311++G(3df) calculations support the assignment of these bands to *nl*-CuC_3 ($X\ ^2A'$) (**G**). However, the B3LYP/6−311++G(3df) calculation gives considerably poorer results. The maximum differences between experimental and predicted isotopomer frequencies, $\nu_{exp} - \omega_{sc}$, are 4.3 cm^{-1} (B3LYP/6−311++G(3df)) and 1.6 cm^{-1} (MPW1PW91/6−311++G(3df)). The average values of these differences for all observed isotopomers (for both modes) are 2.1 and 0.96 cm^{-1}, respectively. Although the 1.6 and 0.96 cm^{-1} values (MPW1PW91) are typical for structures assigned using isotopic ^{13}C labeling, the 4.3 and 2.1 cm^{-1} (B3LYP) values are unacceptably large.

Figure 3 shows that in the 1200 cm^{-1} range only two isotopomer bands (labeled **a** and **c**) appear, while eight appear for the higher frequency mode. To understand this requires looking at the integral intensities of the **c** and **d** isotopomers for both modes (Table 3). MPW1PW91 calculations predict that the integral intensities for the asymmetric and symmetric C═C stretching modes in the **c** isotopomer are 158 and 32 km/mol, while in **d** they are 176 and 26 km/mol, respectively. Thus, for the **c** isotopomer, the intensity ratio of the upper to the lower frequency band is expected to be ≈4.9 (=158/32), which is very close to the observed ratio of the 1788.1 cm^{-1} to 1246.3 cm^{-1} bands. But, for the **d** isotopomer, the predicted ratio is ≈6.8 (=176/26), so the lower frequency band should be substantially weaker. Its absence is thus understandable.

Information about the mechanism of formation of CuC_3 can be obtained from a comparison of the isotopomeric band pattern

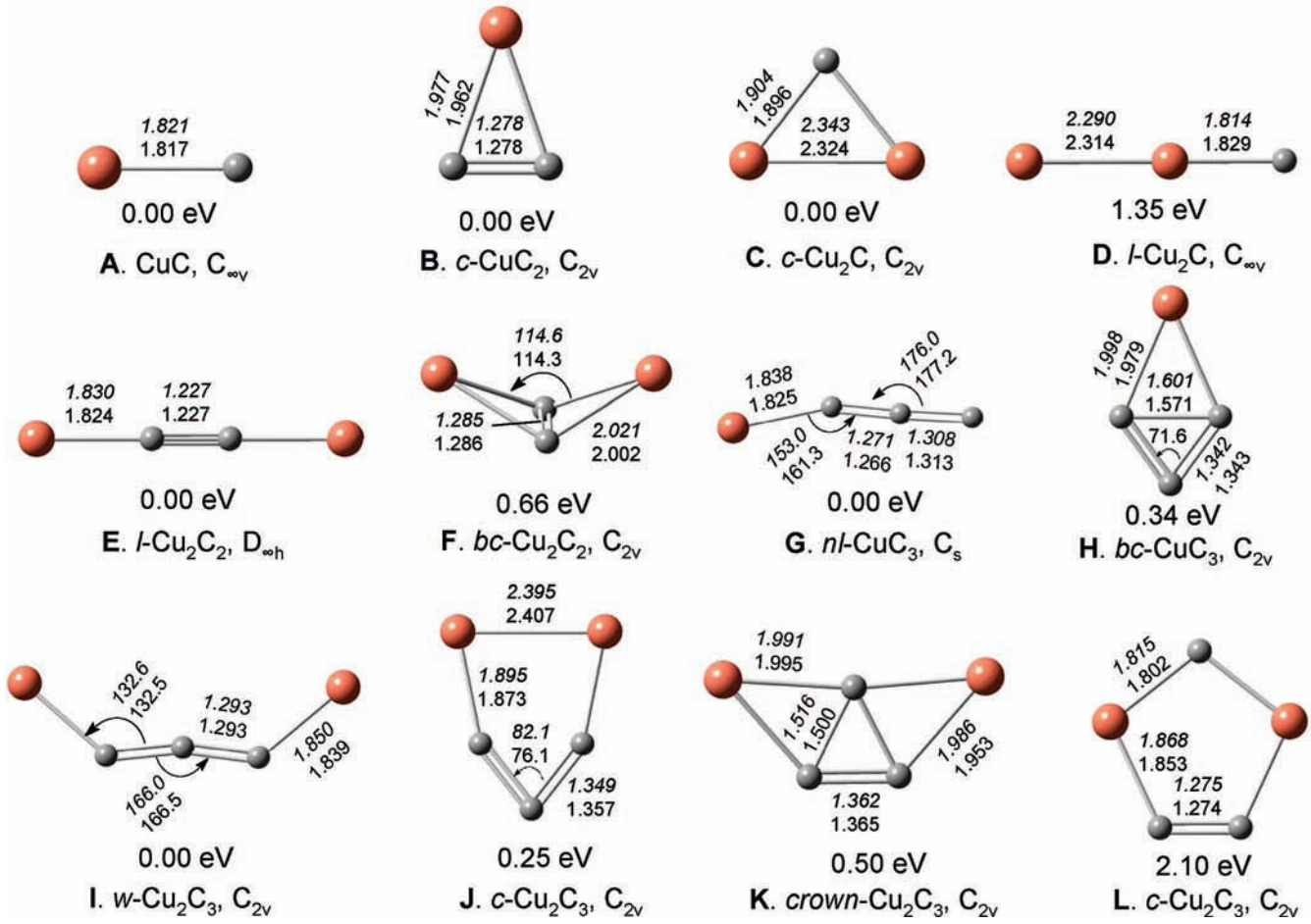

Figure 4. Optimized equilibrium structures for the CuC, CuC_2, Cu_2C, Cu_2C_2, CuC_3, and Cu_2C_3 clusters. The bond lengths (angstroms) and angles (degrees) calculated at B3LYP/6−311++G(3df) (italic type, top) and at MPW1PW91/6−311++G(3df) (normal type) are marked. The relative isomer energies are indicated.

TABLE 1: Vibrational Frequencies (cm^{-1}) and Integral Intensities (km/mol) for Electronic Ground States of Cu_mC_n ($m = 1, 2$; $n = 1, 2, 3$) Clusters (Displayed in Figure 4), Calculated Using B3LYP and MPW1PW91 Functionals

Cu_mC_n Isomer	B3LYP/6−311++G(3df)	MPW1PW91/6−311++G(3df)
A. CuC ($X\ ^4\Sigma$)	σ 572.5 (10)	σ 585.6 (14)
B. *c*-CuC_2 ($X\ ^2A_1$)	a_1 1750.3 (7), a_1 436.4 (5), b_2 291.1(0)	a_1 1768.7 (5), a_1 449.3 (5), b_2 321.9 (0)
C. *c*-Cu_2C. ($X\ ^3A_2$)	a_1 528.3 (6), b_2 389.7 (5), a_1 210.2 (1)	a_1 534.1 (6), b_2 392.4 (7), a_1 218.9 (1)
D. *l*-Cu_2C ($X\ ^3\Sigma_g$)	σ 665.0 (7), π 240.3 (2 × 26), σ 232.7 (5)	σ 574.5 (0), π 509.1 (474), σ 210.1 (1), π 67.3 (0)
E. *l*-Cu_2C_2 ($X\ ^1\Sigma_g$)	σ_g 2093.1 (0), σ_u 659.3 (61), π_g 255.7 (2 × 0), σ_g 254.9 (0), π_u 98.2 (2 × 50)	σ_g 2112.0 (0), σ_u 662.2 (65), π_g 260.5 (2 × 0), σ_g 257.5 (0), π_u 98.4 (2 × 56)
F. *bc*-Cu_2C_2 ($X\ ^1A_1$)	a_1 1703.4 (10), b_2 497.2 (17), a_1 313.2 (21), a_2 140.1 (0), b_1 133.4 (9), a_1 57.8 (14)	a_1 1713.8 (8), b_2 518.3 (23), a_1 324.9 (23), a_2 201.9 (0), b_1 166.1 (10), a_1 51.1 (16)
G. *nl*-CuC_3 ($X\ ^2A'$)	a′ 1901.0 (134), a′ 1272.6 (9), a′ 453.6 (21), a′ 364.3 (23), a″ 228.4 (9), a′ 118.8 (15)	a′ 1900.5 (172), a′ 1281.5 (31), a′ 432.0 (2), a″ 363.3 (28), a″ 227.5 (10), a″ 84.5 (17)
H. *bc*-CuC_3 ($X\ ^2A_1$)	a_1 1595.8 (25), b_2 1208.2 (19), a_1 634.5(22), a_1 351.6 (13), b_1 241.5(7), b_2 189.7 (2)	a_1 1618.3 (13), b_2 1221.9 (21), a_1 729.5 (5), a_1 372.2 (12), b_1 240.1(7), b_2 220.2 (1)
I. *w*-Cu_2C_3 ($X\ ^1A_1$)	b_2 1776.1 (404), a_1 1299.8 (9), a_1 567.2 (3), b_2 536.0 (35), a_1 314.8 (7), b_1 272.9 (3), a_2 241.6 (0), b_2 105.5 (135), a_1 50.2 (7)	b_2 1776.4 (437), a_1 1313.1 (7), a_1 570.3 (2), b_2 548.6 (21), a_1 322.9 (11), b_1 275.6 (4), a_2 240.4 (0), b_2 87.8 (137), a_1 47.5 (8)
J. *c*-Cu_2C_3 ($X\ ^1A_1$)	a_1 1488.7 (601), b_2 1287.2 (5), a_1 447.1 (26), b_2 413.2 (18), a_1 381.0 (112), b_1 356.0 (5), a_2 190.0 (0), a_1 186.7(6), b_2 168.6 (18)	a_1 1521.2 (552), b_2 1267.8 (11), a_1 469.9 (126), a_1 457.6 (136), b_2 411.5 (8), b_1 348.3 (6), a_2 198.5 (0), a_1 171.8 (15), b_2 144.8 (23)
K. *crown*-Cu_2C_3 ($X\ ^1A_1$)	a_1 1471.1 (26), a_1 842.9 (134), b_2 725.9(37), b_2 390.1 (55), a_1 300.6 (9), a_2 258.8 (0), b_2 221.6 (0), b_2 179.8 (18), a_1 90.3 (2)	a_1 1498.4 (11), a_1 906.8 (127), b_2 804.3(3), b_2 425.1 (42), a_1 319.4 (14), b_2 258.3 (0), a_2 256.8 (0), b_1 176.4 (17), a_1 97.2 (2)
L. *c*-Cu_2C_3 ($X\ ^1A_1$)	a_1 1748.1 (87), b_2 638.3 (2), a_1 592.8 (9), a_1 545.4 (20), b_2 539.9 (2), a_2 239.6 (0), b_1 210.3 (23), a_1 129.9 (1), b_2 109.7 (44)	a_1 1766.6 (90), b_2 658.9(2), a_1 605.6 (10), a_1 559.1 (21), b_2 557.6 (3), a_2 228.0 (0), b_1 206.4 (26), a_1 120.6 (1), b_2 70.2 (46)

observed for CuC_3 versus that for C_3. The C_3 isotopomers (and relative band intensities) observed (but not displayed) in the present work were 12-12-12 (1.0), 12-12-**13** (0.46), **13**-12-**13** (0.09), 12-**13**-12 (0.28), **13**-**13**-12 (0.20), and **13**-**13**-**13** (0.11). The CuC_3 isotopomers observed (and shown in Figure 3 and listed in Table 3) were **a** (63-12-12-12) (1.0), **b** (63-12-12-**13**)

TABLE 2: Calculated Total Energies, E_{ZPE} (Hartrees), Corrected for Zero Point Vibrational Energies, And Estimated Dissociation Energies, D_0 (eV) or Isomerization Energy Barriers, E_{Iso}(eV) for Cu_mC_n (n = 1, 2; m = 1, 2, 3) Isomers

Cu_mC_n Isomer	B3LYP/6−311++G(3df)	MPW1PW91/6−311++G(3df)
A CuC ($X\ ^4\Sigma$)	E_{ZPE} = −1678.402 951 D_0 (Cu ($X\ ^2S_{1/2}$) + C ($X\ ^3P$)) = 1.99 eV	E_{ZPE} = −1678.468 587 D_0 (Cu ($X\ ^2S_{1/2}$) + C ($X\ ^3P$)) = 2.20 eV
B *c*-CuC_2 ($X\ ^2A_1$)	E_{ZPE} = −1716.545 045 D_0 (Cu ($X\ ^2S_{1/2}$) + C_2 ($X\ ^1\Sigma_g^+$)) = 2 × 2.33 eV	E_{ZPE} = −1716.594 551 D_0 (Cu ($X\ ^2S_{1/2}$) + C_2 ($X\ ^1\Sigma_g^+$)) = 2 × 2.47 eV
C. *c*-Cu_2C ($X\ ^3A_2$)	E_{ZPE} = −3318.959 383 D_0 (Cu ($X\ ^2S_{1/2}$) + CuC ($X\ ^4\Sigma$)) = 2.29 eV	E_{ZPE} = −3319.095 577 D_0 (Cu ($X\ ^2S_{1/2}$) + CuC ($X\ ^4\Sigma$)) = 2.21 eV
D *l*-Cu_2C ($X\ ^3\Sigma_g$)	E_{ZPE} = −3318.885 540 D_0 (Cu ($X\ ^2S_{1/2}$) + CuC ($X\ ^4\Sigma$)) = 0.28 eV	E_{ZPE} = −3319.045 993 D_0 (Cu ($X\ ^2S_{1/2}$) + CuC ($X\ ^4\Sigma$)) = 0.86 eV
E *l*-Cu_2C_2 ($X\ ^1\Sigma_g$)	E_{ZPE} = −3357.146 742 D_0 (2Cu ($X\ ^2S_{1/2}$) + C_2 ($X\ ^1\Sigma_g^+$)) = 2 × 4.09 eV.	E_{ZPE} = −3357.269 606 D_0 (2Cu ($X\ ^2S_{1/2}$) + C_2 ($X\ ^1\Sigma_g^+$)) = 2 × 4.23 eV
F *bc*-Cu_2C_2 ($X\ ^1A_1$)	E_{ZPE} = −3357.117 387 D_0 (2Cu ($X\ ^2S_{1/2}$) + C_2 ($X\ ^1\Sigma_g^+$)) = 4 × 1.85 eV	E_{ZPE} = −3357.245 412 D_0 (2Cu ($X\ ^2S_{1/2}$) + C_2 ($X\ ^1\Sigma_g^+$)) = 4 × 1.95 eV
G *nl*-CuC_3 ($X\ ^2A'$)	E_{ZPE} = −1754.623 580 D_0 (Cu ($X\ ^2S_{1/2}$) + C_3 ($X\ ^1\Sigma_g^+$)) = 2.07 eV	E_{ZPE} = −1754.655 782 D_0 (Cu ($X\ ^2S_{1/2}$) + C_3 ($X\ ^1\Sigma_g^+$)) = 2.26 eV
H *bc*-CuC_3 ($X\ ^2A_1$)	E_{ZPE} = −1754.600 074 E_{Iso} (*bc*-CuC_3 ($X\ ^2A_1$) → *nl*-CuC_3 ($X\ ^2A'$)) = 0.59[a] eV	E_{ZPE} = −1754.643 139 E_{Iso} (*bc*-CuC_3($X\ ^2A_1$) → *nl*CuC_3($X\ ^2A'$)) = 0.91[b] eV
I *w*-Cu_2C_3 ($X\ ^1A_1$)	E_{ZPE} = −3395.164 221 D_0 (Cu($X\ ^2S_{1/2}$) + *nl*-CuC_3 ($X\ ^2A'$)) = 1.86 eV	E_{ZPE} = −3395.269 749 D_0 (Cu($X\ ^2S_{1/2}$) + *nl*CuC_3($X\ ^2A'$)) = 1.85 eV
J *c*-Cu_2C_3 ($X\ ^1A_1$)	E_{ZPE} = −3395.145 764 D_0 (Cu($X\ ^2S_{1/2}$) + *bc*-CuC_3 ($X\ ^2A_1$)) = 2.00 eV	E_{ZPE} = −3395.260 406 D_0 (Cu($X\ ^2S_{1/2}$) + *bc*-CuC_3 ($X\ ^2A_1$)) = 1.94 eV
K *crown*-Cu_2C_3($X\ ^1A_1$)	E_{ZPE} = −3395.127 280 D_0 (Cu($X\ ^2S_{1/2}$) + *bc*-CuC_3 ($X\ ^2A_1$)) = 1.50 eV	E_{ZPE} = −3395.251 558 D_0 (Cu($X\ ^2S_{1/2}$) + *bc*-CuC_3($X\ ^2A_1$)) = 1.70 eV
L *c*-Cu_2C_3($X\ ^1A_1$)	E_{ZPE} = −3395.085 801 D_0 (*c*-Cu_2C ($X\ ^3A_2$) + C_2 ($X\ ^1\Sigma_g^+$)) = 2 × 3.06 eV	E_{ZPE} = −3395.193 157 D_0 (*c*-Cu_2C ($X\ ^3A_2$) + C_2 ($X\ ^1\Sigma_g^+$)) = 2 × 3.14 eV

[a] Relative energy of TS($^2A'$) in Figure 5 is 1.23 eV when calculated at the B3LYP/6−311++G(3df) level. [b] See the PES of Figure 5.

(≈0.12) + **d** (63-**13**-12-12) (0.29), **f** (63-**13**-12-**13**) (0.08), **c** (63-12-**13**-12) (0.29), **e** (63-12-**13**-**13**) (0.06) + **g** (63-**13**-**13**-12) (0.12), and **h** (63-**13**-**13**-**13**) (0.11). After summing the indicated band absorbances (because the same assumed $^{12/13}C_3$ reactant leads to the (**b**, **d**) and (**e**, **g**) product pairs), the observed isotopomer band pattern of $Cu^{12/13}C_3$ is very similar to the intensity pattern in $^{12/13}C_3$. We can thus conclude that Cu atoms react with already-formed C_3 molecules to form CuC_3.

This conclusion is supported by annealing and photolysis results. Matrix annealing (to 35 K), followed by cooling back to 12 K, increases the intensities of the 1830.0 and 1250.5 cm^{-1} bands by ∼27%. This suggests that Cu ($X\ ^2S_{1/2}$) reacts with C_3 ($X\ ^1\Sigma_g^+$) as a result of diffusion at higher matrix temperatures. Photolysis for 1 h with photon energies of $h\nu \leq 5.5$ eV reduced both the 1830.0 and the 1250.5 cm^{-1} bands by ∼13%. The predicted lowest energy photodissociation path is *nl*-CuC_3 + $h\nu$ → Cu + *l*-C_3, with a dissociation energy of 2.07 eV (2.26 eV) (cf. Table 2). This is close to the calculated Cu−C bond energy of 1.99 eV (2.20 eV) [B3LYP (MPW1PW91)] for diatomic CuC.

4.2.6. Cu_2C_3. Four stable C_{2v} isomers were found on the singlet Cu_2C_3 potential surface. The lowest energy one is w-shaped (**I**) and the other, less stable ones (**J**, **K**, and **L**) are either cyclic or crown-shaped. Again, the large difference in stability between **I** and **K** for B3LYP and MPW1PW91 functionals is reflected in large frequency differences predicted for the three highest energy modes and in the mismatch of the fundamental mode symmetries of **K**, as listed in Table 1. The most intense mode predicted for **I** is 1776.4 cm^{-1} (437 km/mol), the asymmetric CC stretch. No bands assignable to **I** or **J**, **K**, **L** clusters have been observed in this energy region.

4.3. $^{12/13}$C-Isotope Scrambling in the *nl*-CuC_3 Clusters. Since the **b** (63-12-12-**13**) and **d** (63-**13**-12-12) isotopomers originate from the same singly substituted isotopic C_3 precursor (**13**-12-12), Cu might be expected to bond to either chain end with equal probability. If so, it follows that the **b** and **d** isomers should have about the same infrared intensities. Theoretical predictions roughly affirm this expectation. The **d** isomer is predicted to be about 5% more intense than **b**. But, as can be seen in Figure 3, this is not what is observed. The intensity of the **d** band is approximately twice the intensity of the **b** band. A similar argument can be made for the doubly substituted isomers, **e** (63-12-**13**-**13**) and **g** (63-**13**-**13**-12; see Figure 3). **g** is observed to be approximately twice as intense as **e**.

This anomaly is the result of photoscrambling. For background information, we first consider a similar observation in $^{12/13}C_3$ that was also ascribed to isotopic photoscrambling.[36] In $^{12/13}C_3$, scrambling requires photon energies in the 2.75−3.54 eV range (covering the $\tilde{a}^3\Pi_u$ ($^3\Pi$) ← $\tilde{A}^1\Pi_u$ ← $X^1\Sigma_g^+$ transition).[36] The maximum barrier to the forward and backward reactions along the $\tilde{a}^3\Pi_u$ ($^3\Pi$) ↔ TS ($^3A'$) ↔ $^3A'_2$ ↔ TS ($^3A'$) ↔ $\tilde{a}^3\Pi_u$ ($^3\Pi$) reaction pathway has been computed (using full configuration interaction) by Fueno and Taniguchi[37] as 2.82 eV. Visible/UV photolysis of C_3 induces intramolecular rearrangement to a cyclic C_3 intermediate. This is followed by specific bond breaking which leads to a gain in the 12-**13**-12 and 12-**13**-**13** isomer concentrations. This increase results because these isomers have lower zero point energies (ZPE) than their precursors (12-12-**13** or **13**-12-**13**). The observation of isotopic scrambling in C_3 supports the existence of the $^3A'$ transition state and the intermediate triplet cyclic C_3 ($^3A'_2$) structure predicted by Fueno and Taniguchi.[37]

We now consider the photoinduced isotopic scrambling in CuC_3 clusters. Because photoscrambling in C_3 involves a cyclic intermediate, a reaction pathway between **G** and **H** was sought theoretically. The calculated PES (MPW1PW91/6−311++G(3df)) for the Cu-12-12-**13** and Cu-**13**-12-12 isomers is displayed in Figure 5. The angle α ($C_1C_2C_3$) was incremented from 71.6° to 180° and, at each step, all other structural parameters were fully optimized. Starting from the left **G** isomer, the PES rises 1.25 eV to a transition state, TS, and then falls to the **H** isomer, which lies 0.34 eV above **G**. The structural parameters for **G** and **H** are given in Figure 3 and, for the TS, are $R(C_1C_2) = 1.2975$ Å, $R(C_2C_3) = 1.3238$

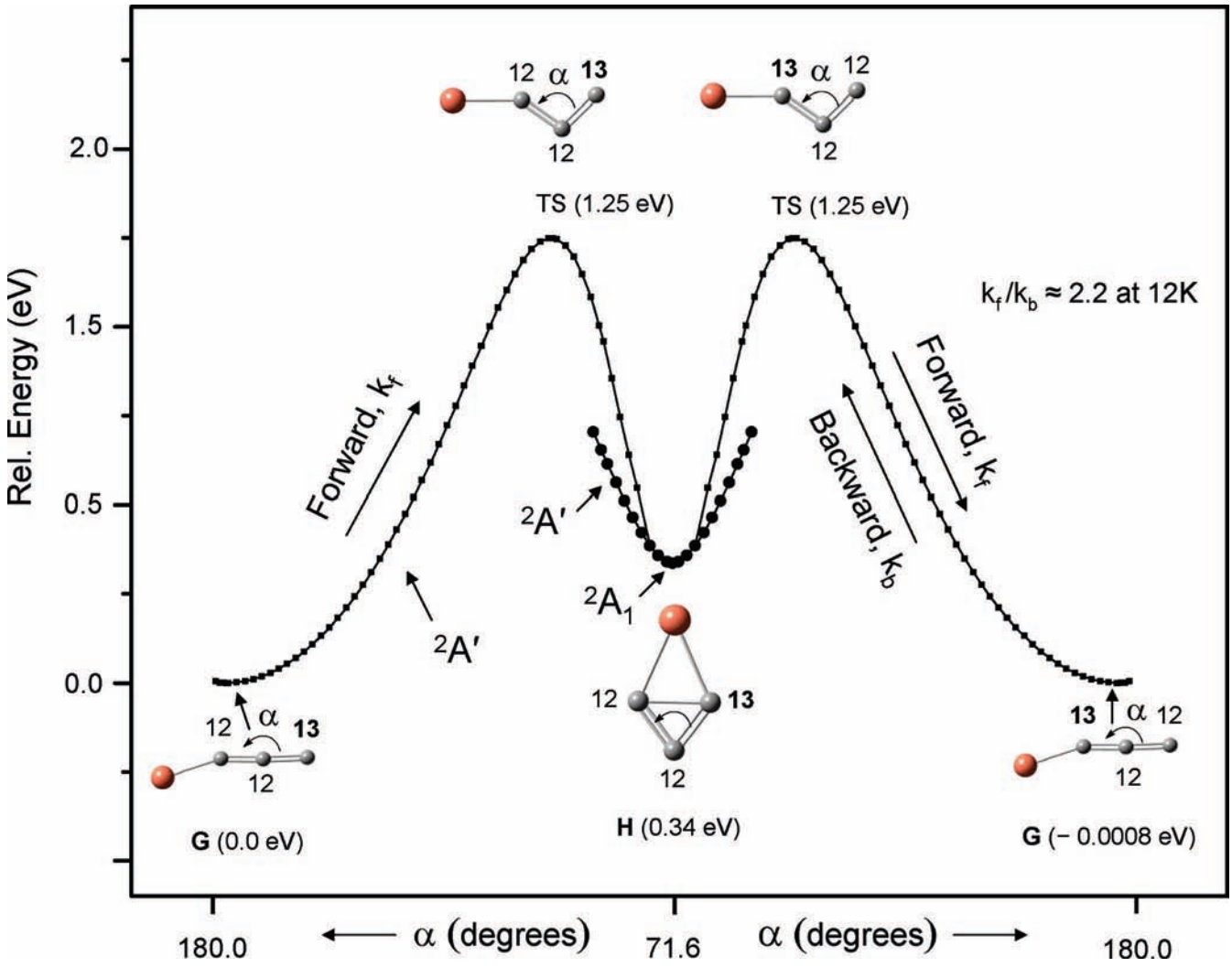

Figure 5. Total energy plot for the near linear CuC_3 ($^2A'$) and bicyclic CuC_3 ($^2A'$ and $^2A'/^2A_1$) clusters calculated at the MPW1PW91/6−311++G(3df) level by incrementing the α (CCC) angle in the range of $77 \leq \alpha \leq 180°$ and $71.6 \leq \alpha \leq 93°$, respectively. For each α, the four remaining geometrical parameters were fully optimized. Note that the 63-12-12-**13** cluster reactant (left) rearranges to the 63-**13**-12-12 lower energy isotopomer product by breaking the $^{12}C-Cu$ bond in structure **H**, then passing over the TS and relaxing to the **G** product (right) in the forward reaction pathway.

Å, $R(C_3Cu) = 1.8537$ Å, $\alpha(C_1C_2C_3) = 100.46°$ and $\beta(CuC_3C_2) = 144.3°$. At $\alpha = 77°$, the $^2A'$ energy surface (small squares in Figure 5) intersects with the **H** isomer distortion PES (large filled circles). The latter has a stable minimum at $\alpha = 71.6°$. For the two curves calculated between $\alpha > 77°$ and 93°, the lower one ($^2A'$) almost preserves the C_{2v} symmetry of the **H** isomer, although it was calculated using C_s symmetry. The bond lengths found show that $R(C_1C_2) \approx R(C_2C_3)$ and $R(CuC_1) \approx R(CuC_3)$. However, for the higher energy curve ($^2A'$), the CC bond length differences increase, that is, $R(C_1C_2) - R(C_2C_3) = 0.01 - 0.03$ Å and the CuC bond lengths differences become large. At $\alpha = 180°$, CuC_3 is linear but exhibits one imaginary frequency (-61 cm^{-1}). The calculated barrier to linearity for the **G** isomer is so much smaller (39 cm^{-1}) than its computed vibrational frequencies (cf. Table 1), that the *nl*-CuC_3 (**G**) isomer can be characterized as quasilinear.

The isotopic scrambling can most easily be tracked by following a specific *nl*-CuC_3 isotopomer on the PES in Figure 5. First, consider the 63-12-12-**13** isotopomer **G** as the reactant. To drive the photoscrambling reaction, the **G** isomer must first absorb a photon and become electronically excited. From the doublet excited state, reversion to the ground-state occurs partially by energy dissipation into the matrix bath modes and partially by internal conversion to the ground electronic state. After internal conversion, the **G** isomer presumably retains sufficient thermal energy to surmount the ground-state TS barrier, thus converting to the **H** isomer. The ^{13}C atom will now be located on the right-hand side of **H** (see Figure 5). Further irradiation may either convert it back to the left **G** isomer (by breaking the just-formed $Cu-^{13}C$ bond) or lead it to the right **G** isotopomer (by breaking the $Cu-^{12}C$ bond). Either reaction is equally probable. If the latter reaction occurs, the 63-**13**-12-12 isotopomer will be formed, and the ^{13}C isotope position will have been scrambled. If the former reaction occurs, no scrambling will have occurred, and reversion to the initial reactant ensues. Backward reactions from the right isotopomer (through **H** to the left **G**) could then occur. The relative rates of the forward and backward rates are dependent on the energy differences of the two stable **G** isotopomers and may be calculated.

The ratio of the forward-to-backward reaction rate constants, under thermal equilibrium conditions, can be described by

TABLE 3: Experimental (Ar Matrix, 12 K) and Calculated Isotopomer Frequencies (Integral Intensities) for the Asymmetric and Symmetric CC Stretch Fundamental Modes of Fully Optimized Equilibrium Geometry of Near-Linear $^{63}Cu^{12/13}C$ (G, Figure 4)[a]

Asymmetric CC stretch mode			B3LYP/6−311++G(3df)		MPW1PW91/6−311++G(3df)	
	Isotopomer	ν_{exp}/cm^{-1}	ω_{sc}[b]/cm^{-1}(km/mol)	$\nu_{exp} - \omega_{sc}$/cm^{-1}	ω_{sc}[c]/cm^{-1}(km/mol)	$\nu_{exp} - \omega_{sc}$/cm^{-1}
a	63-12-12-12	1830.0	1830.0 (134)	0.0	1830.0 (171)	0.0
b	63-12-12-**13**	1825.5	1824.2 (131)	1.3	1825.5 (168)	0.0
c	63-12-**13**-12	1788.1	1785.2 (125)	2.9	1786.6 (158)	1.5
d	63-**13**-12-12	1807.6	1810.4 (134)	−2.8	1807.7 (176)	−0.1
e	63-12-**13**-**13**	1783.8	1779.5 (123)	4.3	1782.2 (154)	1.6
f	63-**13**-12-**13**	1802.4	1803.8 (132)	−1.4	1802.6 (172)	−0.2
g	63-**13**-**13**-12	1764.4	1764.5 (125)	−0.1	1763.1 (162)	1.3
h	63-**13**-**13**-**13**	1759.5	1758.0 (123)	1.5	1758.0 (158)	1.5
Symmetric CC stretch mode						
a	63-12-12-12	1250.5	1250.5 (9)	0.0	1250.5 (31)	0.0
b	63-12-12-**13**		1224.6 (9)		1224.2 (32)	
c	63-12-**13**-12	1246.3	1248.7 (9)	−2.4	1247.8 (32)	−1.5
d	63-**13**-12-12		1228.4 (7)		1229.7 (26)	
e	63-12-**13**-**13**		1222.3 (10)		1220.8 (33)	
f	63-**13**-12-**13**		1202.9 (8)		1203.9 (27)	
g	63-**13**-**13**-12		1249.0 (7)		1227.9 (27)	
h	63-**13**-**13**-**13**		1222.6 (8)		1201.4 (28)	

[a] Proposed band assignments marked in Figure 3 are given in the first column. [b] Frequencies are scaled uniformly by a scaling factor of 0.9627 for the asymmetric mode and 0.9826 for the symmetric mode. [c] Frequencies are scaled uniformly by a scaling factor of 0.9629 for the asymmetric mode and 0.9758 for the symmetric mode.

$$k_f/k_b = \exp(-\triangle G/kT) \quad (1)$$

where ΔG is the difference in the Gibbs free energy of products and reactants, k is the Boltzmann constant, and T is the sample temperature.[40] At low temperatures (as in a matrix), it may be assumed that the changes in entropy are small, thus $\Delta G = \Delta E_{ZPE}$ Equation 1 can then be rewritten

$$k_f/k_b = \exp(-\triangle E_{ZPE}/kT) \quad (2)$$

The energy of the 63-13-12-12 isotopomer is lower than the 63-12-12-13 isotopomer by 6.6 cm^{-1} (MPW1PW91/6−311++G (3df)). Thus, $\Delta E_{ZPE} = -6.6$ cm^{-1} and the ratio of the forward and reverse rate constants, estimated from eq 2, is ≈2.2 (at 12 K). Thus, the concentration of the 63-**13**-12-12 isotopomer **d** will increase at the expense of the 63-12-12-**13** isotopomer **b**, as observed in Figure 3.

A similar procedure can be applied to the 63-**13**-**13**-12 product and 63-12-**13**-**13** reactant isotopomers. Again, ΔE_{ZPE} was found to be $= -6.6$ cm^{-1} and $k_f/k_b \approx 2.2$ (at 12 K). Thus, the 63-**13**-**13**-12 isotopomer **g** is expected to increase, while 63-12-**13**-**13** isotopmer **e** should decrease, again as observed.

The photo-induced $^{12/13}$C-isotopic scrambling effect in CuC_3 could be applicable to those clusters potentially formed in interstellar space, in the gas phase and/or trapped on cold grain surfaces. The scrambling reactions could be driven by the absorption of stellar UV−visible radiation or cosmic radiation which penetrates even to dark and cold nebular interiors. Such scrambling will yield isotopic fractionation in $^{63}Cu^{12/13}C_3$ clusters via the reactions described here.

5. Conclusions

After the ablation and trapping of copper and carbon in an argon matrix, new infrared absorption bands were observed at 1830.0 and 1250.5 cm^{-1}. These bands have been assigned to the two most intense modes, that is, the asymmetric and symmetric C═C stretches, of the Cu-carbon cluster, *nl*-$^{63}CuC_3$. This assignment was supported by calculations using density functional theory with MPW1PW91 functional and 6−311++G (3df) basis set. The MPW1PW91/6−311++G (3df) approach predicts the relative integral intensities for these modes quite well. However, the BPW91/6−311++G(3df) [carbons]// SDD pseudopotentials [Cu] and B3LYP/6−311++G(3df) calculations failed to correctly predict the ^{13}C-labeled infrared isotopomer frequencies and the relative integral intensities for those modes.

The photoinduced isotopic scrambling in $^{63}Cu^{12/13}C_3$ isotopomers was observed and explained via a computed (MPW1PW91/6−311++G(3df)) PES for this reaction. The forward reactions of **G** → **G***→ TS → **H** → TS → **G** indicates that scrambling in the isotopomers 63-12-12-**13** (**b**) → 63-**13**-12-12 (**d**) and 63-12-**13**-**13** (**e**) → 63-**13**-**13**-12 (**g**) occurs via the bicyclic **H** isomer. At 12 K, the estimated forward rate constant (k_f) is 2.2 times larger than the backward rate constant (k_b), so the accumulation of 63-**13**-12-12 and 63-**13**-**13**-12 isotopomers is expected during matrix photolysis, exactly as observed.

A number of pure carbon clusters larger than C_3, seen in Figure 2, were formed in the present experiments. Many bands, mainly in the 1775−1900 cm^{-1} range, in Figure 2b have been left unassigned. It is likely that many are due to products of reactions of larger carbon clusters with copper. We plan to extend our studies to larger Cu/carbon clusters and will report on these in the near future.

Acknowledgment. The authors are grateful to The Petroleum Research Fund, administered by the American Chemical Society, for its support of this research.

References and Notes

(1) De Boer, K. S.; Lamers, H. J. G. L. M. *Astron. Astrophys.* **1978**, *69*, 327.
(2) Savage, B. D.; Bohlin, R. C. *Astrophys. J.* **1979**, *229*, 136.
(3) Jenkins, E. B.; Savage, B. D.; Spitzer, L. *Astrophys. J.* **1986**, *301*, 355.
(4) Szczepanski, J.; Wang, H.; Vala, M.; Tielens, A. G. G. M.; Eyler, J. R.; Oomens, J. *Astrophys. J.* **2006**, *646*, 666.
(5) The NASA Imagine Team What is your Cosmic Connection to the Elements 1997, http://imagine.gsfc.nasa.gov/docs/teachers/elements/imagine/cont nts.html, 08/2005.

(6) Robbins, D. L.; Rittby, C. M. L.; Graham, W. R. M. *J. Chem. Phys.* **2001**, *114*, 3570.
(7) Kinzer, R. E., Jr.; Rittby, C.; M., L.; Graham, W. R. M. *J. Chem. Phys.* **2006**, *125*, 074513.
(8) Bates, S. A.; Rittby, C. M. L.; Graham, W. R. M. *J. Chem. Phys.* **2006**, *125*, 074506.
(9) Bates, S. A.; Rhodes, J. A.; Rittby, C. M. L.; Graham, W. R. M. *J. Chem. Phys.* **2007**, *127*, 064506.
(10) Kinzer, R. E.; Rittby, C. M. L.; Graham, W. R. M. *J. Chem. Phys.* **2008**, *128*, 064312.
(11) Datta, B. P.; Raman, V. L.; Subbanna, C. S.; Jain, H. C. *Int. J. of Mass Spectrometry and Ion Processes* **1989**, *91*, 241.
(12) Guo, B. C.; Kerns, K.; Castleman, A. W., Jr *Science* **1992**, *255*, 1411.
(13) Kosolapova, T. Y. *Carbide*; Plenum Press: New York, 1971.
(14) Katskov, D. A.; Kruglikova, L. P.; L'vov, B. V.; Polzik, L. K. *Zh. Prikl. Spektrosk.* **1976**, *25*, 918; *J. Appl. Spectry. [USSR]* **1976**, *25*, 1459.
(15) Yamada, Y.; Castleman, A. W., Jr. *Chem. Phys. Lett.* **1993**, *133*, 204.
(16) Fowles, G. R. *Introduction to Modern Optics*; Dover Publications Inc.: New York, 1975.
(17) Frisch, M. J.; Trucks, G. W.; Schlegel, H. B.; Scuseria, G. E.; Robb, M. A.; Cheeseman, J. R.; Montgomery, Jr. J. A.; Vreven, T.; Kudin, K. N.; Burant, J. C., Millam, J. M.; Iyengar, S. S.; Tomasi, J.; Barone, V.; Mennucci, B.; Cossi, M.; Scalmani, G.; Rega, N.; Petersson, G. A.; Nakatsuji, H.; Hada, M.; Ehara, M.; Toyota, K.; Fukuda, R.; Hasegawa, J.; Ishida, M.; Nakajima, T.; Honda, Y.; Kitao; O.; Nakai, H.; Klene, M.; Li, X.; Knox, J. E.; Hratchian, H. P.; Cross, J. B.; Bakken, V.; Adamo, C.; Jaramillo, J.; Gomperts, R.; Stratmann, R. E.; Yazyev, O.; Austin, A. J.; Cammi, R.; Pomelli, C.; Ochterski, J. W.; Ayala, P. Y.; Morokuma, K.; Voth, G. A.; Salvador, P.; Dannenberg, J. J.; Zakrzewski, V. G.; Dapprich, S.; Daniels, A. D.; Strain, M. C.; Farkas, O.; Malick, D. K.; Rabuck, A. D.; Raghavachari, K.; Foresman, J. B.; Ortiz, J. V.; Cui, Q.; Baboul, A. G.; Clifford, S.; Cioslowski, J.; Stefanov, B. B.; Liu, G.; Liashenko, A.; Piskorz, P.; Komaromi, I.; Martin, R. L.; Fox, D. J.; Keith, T.; Al-Laham, M. A.; Peng, C. Y.; Nanayakkara, A.; Challacombe, M.; Gill, P. M. W.; Johnson, B.; Chen, W.; Wong, M. W.; Gonzalez, C.; Pople, J. A. *Gaussian 03, Revision B. 05*; Gaussian, Inc.: Wallingford, CT, 2004.
(18) Becke, A. D. *J. Chem. Phys.* **1993**, *98*, 5648.
(19) Wiberg, K. *J. Comput. Chem.* **1999**, *20*, 1299.
(20) Dunbar, R. *J. Phys. Chem.* **2002**, *106*, 7328.
(21) Oomens, J.; Moore, D. T.; von Helden, G.; Mejier, G.; Dunbar, R. *J. Am. Chem. Soc.* **2004**, *126*, 724.
(22) Wang, Y.; Szczepanski, J.; Vala, M. *Chem. Phys.* **2007**, *342*, 107.
(23) Perdew, J. P.; Wang, Y. *Phys. Rev. B* **1992**, *45*, 132444.
(24) Adamo, C.; Barone, V. J. *Chem. Phys.* **1998**, *102*, 1995.
(25) Legge, F. S.; Nyberg, G. L.; Peel, J. B. *J. Phys. Chem. A* **2001**, *105*, 7905.
(26) Wang, X.; Andrews, L. *Angew. Chem., Int. Ed.* **2003**, *42*, 5201.
(27) Weltner, W., Jr.; Van Zee, R. J. *Chem. Rev.* **1989**, *89*, 1713.
(28) Van Orden, A.; Saykally, R. J. *Chem. Rev.* **1998**, *98*, 2313.
(29) Szczepanski, J.; Auerbach, E.; Vala, M. *J. Phys. Chem.* **1997**, *101*, 9296.
(30) Szczepanski, J.; Hodyss, R.; Vala, M. *J. Phys. Chem.* **1998**, *102*, 8300.
(31) Gutsev, G. L.; Andrews, L.; Bauschlicher, C. W. *Chem. Phys.* **2003**, *290*, 47.
(32) Jacox, M. E.; Milligan, D. E. *Chem. Phys.* **1974**, *4*, 45.
(33) Jiang, Q.; Rittby, C. M. L.; Graham, W. R. M. *J. Chem. Phys.* **1993**, *99*, 3194.
(34) Szczepanski, J.; Ekern, S.; Vala, M. *J. Phys. Chem.* **1995**, *99*, 8002.
(35) Grotjahn, D. B.; Brewster, M. B.; Ziurysh, M. *J. Am. Chem. Soc.* **2002**, *124*, 5895.
(36) Szczepanski, J.; Vala, M. *Eur. Phys. J.-Special Topics* **2007**, *144*, 27.
(37) Fueno, H.; Taniguchi, Y. *Chem. Phys. Lett.* **1999**, *312*, 65.
(38) Andrews, L.; Kushto, G. P.; Zhou, M.; Wilson, S. P.; Souter, P. F. *J. Chem. Phys.* **1999**, *110*, 4457.
(39) Ding, X. D.; Wang, S. L.; Rittby, C. M. L.; Graham, W. R. M. *J. Chem. Phys.* **2000**, *112*, 5113.
(40) Herbst, E. *Space Sci. Rev.* **2002**, *96*, 1.

JP801111M